Arabian Journal of Chemistry (2023) **16**, 104546

King Saud University

Arabian Journal of Chemistry

www.ksu.edu.sa
www.sciencedirect.com

ORIGINAL ARTICLE

An unexpectedly stable Y_2B_5 compound with the fractional stoichiometry under ambient pressure

Yuanyuan Jin [a], Wenjie Huang [a], Jinquan Zhang [a], Song Li [a], Shubo Cheng [a], Weiguo Sun [b], Meng Ju [c], Chuanzhao Zhang [a,*]

[a] *Department of Physics and Optoelectronic Engineering, Yangtze University, Jingzhou 434023, China*
[b] *College of Physics and Electronic Information, Luoyang Normal University, Luoyang 471022, China*
[c] *School of Physical Science and Technology, Southwest University, Chongqing 400715, China*

Received 25 May 2022; accepted 3 January 2023
Available online 9 January 2023

KEYWORDS

Transition-metal borides;
First-principles calculation;
Fractional stoichiometry;
Structural characteristics;
Vickers hardness

Abstract Boron-rich yttrium borides are an exceptional group of compounds not only with excellent mechanical properties, but also with particular superconducting and thermoelectric properties. Although the Y–B compounds with integral components have been extensively investigated experimentally and theoretically, the yttrium borides with the fractional stoichiometries are rarely observed. Herein, utilizing a combination of the CALYPSO method for crystal structure prediction and first-principles calculations, we made an investigation on a broad range of stoichiometries of yttrium borides. An extraordinary stable Y_2B_5 compound possessing the fractional stoichiometry with the monoclinic $P12_1/c1$ phase is firstly uncovered. Structurally, the $P12_1/c1$-Y_2B_5 crystalline consists of the distorted B_6 octahedrons and seven-member B rings. Remarkably, the B–B covalent network following the increment of the boron content in six concerned yttrium borides undergoes an increasing dimension, quasi one-dimensional chain → two-dimensional B ring → a combination of two-dimensional B ring and three-dimensional B_6 octahedron → three-dimensional B_{24} cage. According to a microscopic hardness model, $P12_1/c1$–Y_2B_5 is considered as an incompressible and hard material with the hardness of 18.83 GPa. More importantly, *Fm*-3 *m*-YB_{12} can be classified into an ultra-incompressible material with the appreciable Vickers hardness of 33.16 GPa. The present consequences can provide important insights for understanding the complex crystal structures of boron-rich yttrium borides and stimulate further experimental synthesis of novel multifunctional materials with the fractional compositions.

* Corresponding author.
E-mail address: zcz19870517@163.com (C. Zhang).

Peer review under responsibility of King Saud University.

Production and hosting by Elsevier

https://doi.org/10.1016/j.arabjc.2023.104546
1878-5352 © 2023 The Author(s). Published by Elsevier B.V. on behalf of King Saud University.

1. Introduction

In the past decades, transition-metal borides (TMBs) have attracted widespread attention because of the high hardness, ultra-compressibility, high melting points, excellent thermal stability and superior electrical properties (Ma et al., 2017; Lu et al., 2020; Liang et al., 2019; Jothi et al., 2018; Levine et al., 2009; Zhang et al., 2012). These highlighted properties make them possess a wide range of applications, for instance, in cutting and polishing tools, coating materials, abrasives, etc (Gu et al., 2021; Cumberland et al., 2005). Among these TMBs, boron rich compounds, have received a lot of attention and are regarded as the potential superhard materials such as ReB_2 (48 GPa by 0.49 N) (Chung et al., 2007), OsB_2 (37 GPa) (Weinberger et al., 2009), CrB_4 (48 GPa) (Niu et al., 2012), WB_4 (43 GPa) (Mohammadi et al., 2011), MnB_4 (35–37 GPa) (Gou et al., 2014) and FeB_4 (62 GPa) (Gou et al., 2013). However, access to boron-rich TMBs with high hardness just by exploring the borides with the integral ratios of B/TM is limited. Thereby, much effort has been devoted to the investigation of the boron-rich TMBs having the fractional stoichiometries. Two promising superhard compounds, $IrB_{1.1}$ and $RhB_{1.1}$ (Latini et al., 2010); experimentally fabricated by applying the pulsed laser deposition technique, have the extraordinarily high hardness values of 43 and 44 GPa, respectively. Subsequent theoretical investigations have further demonstrated that Nb_2B_3 is a superior hard material with a hardness value of 33.5 GPa (Pan and Lin, 2015). Meanwhile, Li *et al*. unveiled two fractional stoichiometries in the Ti–B system, Ti_3B_4 and Ti_2B_3, which possess the calculated hardness values of 32.2 and 33.7 GPa (Li et al., 2015). Recently, W_2B_3 with the $P2_1/m$ symmetry and W_2B_5 having the $R3m$ phase, have been calculated to exhibit the latent ultra-incompressibility with the Vickers hardness values of 31.7 and 36.5 GPa (Zhao et al., 2018). In view of the above descriptions, the boron-rich TMBs with fractional stoichiometries play an important role in designing superhard materials. In consequence, to better disclose more boron-rich TMBs with superhard character, it is earnestly needed to study probe into the boron-rich TMBs not only with the integral ratios but also with the fractional stoichiometries.

The yttrium borides are probably the technologically most important binary system among the transition metal borides. The boron-rich compounds in the Y–B binary system exhibit particular superconducting properties (Xu et al., 2007; Lortz et al., 2006; Wang et al., 2018) and have been considered to be attractive candidates as high temperature thermoelectric materials (Hossain et al., 2015; Sauerschnig et al., 2020). On account of the outstanding properties of boron-rich yttrium borides and their applications in various fields, great efforts have been devoted to probe into them both experimentally and theoretically. So far, five different stoichiometric compositions in the Y–B binary system (YB_2, YB_4, YB_6, YB_{12}, and YB_{66}) have been confirmed from experimental measurements (Liao and Spear, 1995). The YB_2 compound crystallizes into the AlB_2-type structure with space group of $P6/mmm$, which is classified into the hexagonal crystalline system. Song and co-workers (Song et al., 2001) revealed that YB_2 is a paramagnetic compound and the temperature dependence of magnetic susceptibility obeys excellently the Curie-Weiss law above 20 K. For the YB_4 compound, the previous investigations (Villars and Cenzual, 2007; Jäger et al., 2004; Waškowska et al., 2011) uncovered that it has a tetragonal $P4/mbm$ configuration with the high bulk moduli (185 GPa). YB_6 was proposed to possess the cubic $Pm\text{-}3\ m$ phase under ambient pressure, which is similar to CaB6 (Xu et al., 2007; Lortz et al., 2006; Liao and Spear, 1995). Moreover, previous first-principles calculations demonstrated that the most stable phase undergoes a high-pressure phase transition with the transition order of $Pm\text{-}3\ m \rightarrow Cmmm \rightarrow I4/mmm$ with the corresponding transformation pressures of 3.2 and 35.8 GPa (Wang et al., 2018). Very recently, Ding *et al*. discovered a novel $R\text{-}3\ m$ structure of YB_6, which is more stable than the experimentally synthesized $Pm\text{-}3\ m$ phase, with a considerable hardness of 37 GPa (Ding et al., 2021). Consensus has been reached on that the YB_{12} (Shein and Ivanovskǐ, 2003; Czopnik et al., 2005) and YB_{66} (Seybolt, 1960; Richards and Kaspar, 1969; Oliver and Brower, 1971; Günster et al., 1998; Mori and Tanaka, 2006) compounds adopt the cubic $Fm\text{-}3\ m$ and $Fm\text{-}3c$ phases, respectively. Besides the aforementioned five Y–B compounds, the other boron-rich yttrium borides-YB_{25} (Tanaka et al., 1997), YB_{48} (Hossain et al., 2015), YB_{56} (Higashi et al., 1997; Oku et al., 1998), and YB_{62} (Higashi et al., 1997), have also been studied in experiment. However, up to now, few studies have been focused on the crystalline structures of yttrium borides with fractional stoichiometric ratios. Therefore, we aim to corroborate whether there are stable structures with the fractional stoichiometries in the binary Y–B compounds. On the other hand, the rich phase diagram arises another issue: are there novel stable phases of Y–B crystals with unpredictable physical properties could not be uncovered in the preceding research? Consequently, these doubts inspire us to explore whether other stoichiometries of yttrium borides on the boron-rich side could be stable under ambient pressure, especially for the Y–B compounds with the fractional compositions.

In the present work, we comprehensively probe into the stable and metastable phases of yttrium borides with eleven stoichiometries based on an unbiased CALYPSO structural search method in conjunction with first-principles calculations under pressure of 1 atm. In addition, the structural features, mechanical properties, chemical bonding and hardness of typical stable yttrium borides are also systematically predicted. Four experimentally fabricated structures (YB_2, YB_4, YB_6, and YB_{12}) (Song et al., 2001; Jäger et al., 2004; Czopnik et al., 2005) have been successfully reproduced, which substantiate the reasonability of our structure search methodology. Notably, a novel Y_2B_5 compound containing the fractional component with the monoclinic $P12_1/c1$ structure is firstly discovered under atmospheric pressure. This $P12_1/c1$-Y_2B_5 phase possesses the distorted B_6 octahedrons and seven-member B rings. More importantly, as the B content increases, the B–B covalent network exhibits an increasing dimension, namely, quasi one-dimensional chain → two-dimensional B ring → a combination of two-dimensional B ring and three-dimensional B_6 octahedron → three-dimensional B_{24} cage. This phenomenon is firstly uncovered in six considered yttrium borides (YB, YB_2, Y_2B_5, YB_4, YB_6 and YB_{12}). The $P12_1/c1$-Y_2B_5 phase is observed to be an incompressible and hard material with the hardness of 18.83 GPa. More importantly, the $Fm\text{-}3\ m$-YB_{12} structure can be regarded as an ultra-incompressible material with a considerable Vickers hardness of 33.16 GPa.

2. Computational methods

To intensively obtain the stable and metastable crystalline structures of yttrium borides with a variety of compositions (Y_mB_n, m/n = 2/1, 3/2, 1/1, 3/4, 2/3, 1/2, 2/5, 1/3, 1/4, 1/6, and 1/12), we carried out an unbiased structure prediction on the basis of the particle swarm optimization algorithm as implemented in the CALYPSO code (Wang et al., 2010; Wang et al., 2012). This methodology is effectively capable of discovering the stable or metastable phases only relying on the given components, which has been corroborated with the successfully predicted examples from element solid to binary and ternary systems under ambient and high pressures (Lv et al., 2011; Wang et al., 2020; Jin et al. n.d.; Zhang et al., 2017; Zhang et al., 2022; Sun et al., 2020; Chen et al., 2021). The structure predictions were conducted using simulation cells containing up to four formula units (f.u.) at atmospheric pressure. The detailed description on this search algorithm can be found in the related literatures (Wang et al., 2010; Wang et al., 2012).

The subsequent structural optimizations and electronic structure calculations were performed based on density functional theory within the generalized gradient approximation

(GGA) of the Perdew – Burke – Ernzerhof (PBE) exchange–correlation functional, as executed in the Vienna ab initio simulation package (VASP) (Kresse and Furthmüller, 1996; Perdew et al., 1996). Plane-wave basis sets and the projector augmented wave (PAW) method were applied to describe the electron–ion interactions with $4s^24p^65s^24d^1$ and $2s^22p^1$ regarded as valence electrons for Y and B atoms, respectively (Kresse and Joubert, 1999). A kinetic cutoff energy of 800 eV for the expansion of the wave function into plane waves and proper Monkhorst – Pack k-meshes were selected to insure that all the enthalpy calculations were well converged within 1 meV/atom (Monkhorst and Pack, 1976). The formation energy (ΔG), relative to the elemental solids (hexagonal α-Y and rhombohedral α-B with space groups of $P6_3/mmc$ and R-3 m, respectively) (Spedding et al., 1961; Decker and Kasper, 1959), was estimated at atmospheric pressure on the basis of the equation below:

$$\Delta G(Y_mB_n) = [G(Y_mB_n) - mG(Y) - nG(B)]/(m+n) \quad (1)$$

where $G = U + PV - TS$ is the total Gibbs free energy of each composition, and ΔG is the formation energy per atom of the given compound. Herein, G, U, P, V, T and S denote the Gibbs free energy, internal energy, pressure, volume, temperature, and entropy, respectively. It is noted that G reduces to the enthalpy ($H = U + PV$) at 0 K (Feng et al., 2008). The phonon spectra were computed by employing the direct supercell approach as conducted in the Phonopy code (Parlinski et al., 1997; Togo et al., 2008), which aims to verify the dynamical stability of the considered crystal structures. To assess the thermal stability of the considered Y–B compounds, *ab initio* molecular dynamics (AIMD) simulations using NVT (N is the number of particles, V is volume, and T is temperature) ensemble were conducted using the Nosé–Hoover chain thermostat (Martyna et al., 1992) at 300 K for 10 ps with a time step of 2 fs. The crystal orbital Hamilton populations (COHP) and integrated crystal orbital Hamilton populations (ICOHP) are performed as implemented in the LOBSTER code (Dronskowski and Bloechl, 1993; Maintz et al., 2016) to analyze the interatomic interactions. The elastic constants were determined by calculating stress tensor generated by applying a small strain to an optimized unit cell. Moreover, the bulk modulus (B), shear modulus (G), Young's modulus (E), and Poisson's ratio were thus derived from the Voigt – Reuss – Hill (VRH) approximation (Hill, 1952). The hardness of the considered yttrium borides was estimated with the Tian model (Tian et al., 2012).

3. Results and discussion

3.1. Convex hull and phase stability

In the first step, structure searches of solid yttrium and boron were implemented under atmospheric pressure. Remarkably, the well-known hexagonal α-Y ($P6_3/mmc$) (Spedding et al., 1961) and rhombohedral α-B (R-3 m) (Decker and Kasper, 1959) phases observed in experiments for solid yttrium and boron were successfully reproduced within the CALYPSO methodology, confirming the feasibility of our calculations. A following structure prediction on the Y–B compounds with eleven components (Y_2B, Y_3B_2, YB, Y_3B_4, Y_2B_3, YB_2, Y_2B_5, YB_3, YB_4, YB_6, YB_{12}) was made by utilizing the CALYPSO method in combination with first-principles method at ambient pressure. The phase stability at 0 K can be judged based on the formation enthalpy per atom in Y_mB_n, which can be calculated as follows:

$$\Delta H = [H(Y_mB_n) - mH(\text{Solid Y}) - nH(\text{Solid B})]/(m+n) \quad (2)$$

Here, ΔH is the relative formation enthalpy per atom for the yttrium boride with the Y_mB_n composition and E (Y_mB_n) is the total energy per formula unit of this compound. Moreover, E (Solid Y) and E (Solid B) denote the equilibrium enthalpies of each Y and B atom situated in the respective ground state (Spedding et al., 1961; Decker and Kasper, 1959). On the basis of the above formula, the lowest enthalpy structures of each above components in the Y–B binary system were further confirmed, whose crystal structures are depicted in Fig. S1 of the supplementary information with the corresponding structural information summarized in Table S1.

To verify the relative stability of the lowest enthalpy structures of each composition in the Y–B binary system, the convex hull of the Y–B system at 0 K under ambient pressure is constructed in Fig. 1. In addition, the lattice parameters, a, b and c, cell volume per formula unit V, total enthalpies per formula unit H and formation enthalpies per atom ΔH for the lowest formation enthalpy of each compositions of the Y – B binary system are summarized in Table S2. Any phase whose formation enthalpy located exactly on the convex hull is considered as energetically stable, both against decomposition into the elements and into any combination of other binary compounds, and thus synthesizable in principle experimentally (Ghosh and A.van de Walle, M. Asta, , 2008; Zhang et al., 2009). As displayed in Fig. 1, only four compounds sit exactly right on the curves of the convex hull, namely, $P6/mmm$-YB_2, $P12_1/c1$-Y_2B_5, $P4/mbm$-YB_4 and Fm–3 m-YB_{12}, declaring that they are thermodynamically stable. Among them, $P6/mmm$-YB_2, $P4/mbm$-YB_4 and Fm–3 m-YB_{12} have been already fabricated in the laboratory (Song et al., 2001; Jäger et al., 2004; Czopnik et al., 2005); nevertheless, the Y_2B_5 compound with the monoclinic $P12_1/c1$ configuration is a novel ground-state form acquired within our structure search calculations. More

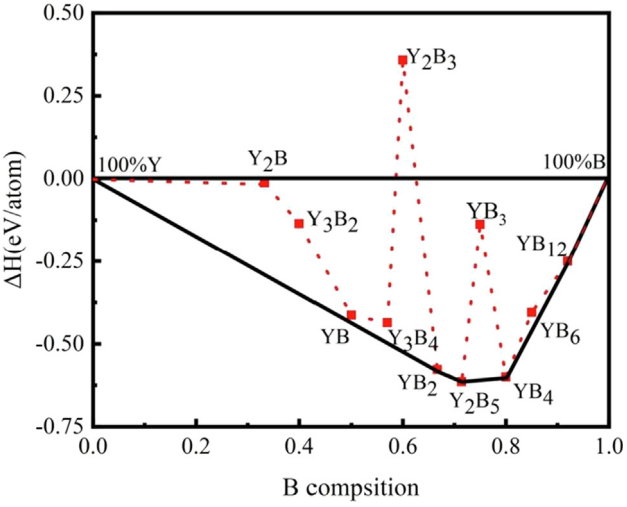

Fig. 1 The convex hull diagram of the Y – B binary system under ambient pressure. The solid line expresses the ground-state convex hull.

importantly, this new structure is a thermodynamically stable phase and possesses an unprecedentedly fractional stoichiometry in the Y–B binary system. Aside from the aforementioned four stable components lying on the convex hull, we also focus on the low-enthalpy metastable phases, which are situated marginally above the convex hull lines. From Fig. 1, the *Cmcm*-YB and *Pm*–3 *m*-YB_6 structures lie above the convex hull by 14 and 17 meV, respectively, which illustrates both compounds could be synthesized under particular temperature and pressure conditions. To further evaluate the thermal contributions to the formation free energy, we constructed the convex hull of the Y–B system under ambient pressure at the temperatures of 300, 1000 and 2000 K, along with that at 0 K, as summarized in Fig. S2. At 300 and 1000 K, the stable compounds are also *P*6/*mmm*-YB_2, $P12_1/c1$-Y_2B_5, *P*4/*mbm*-YB_4 and *Fm*–3 *m*-YB_{12}. Additionally, the *Cmcm*-YB and *Pm*–3 *m*-YB_6 structures also slightly lie above the convex hull. Therefore, *P*6/*mmm*-YB_2, $P12_1/c1$-Y_2B_5, *P*4/*mbm*-YB_4 and *Fm*–3 *m*-YB_{12} are stable and *Cmcm*-YB and *Pm*–3 *m*-YB_6 should be classified into metastable phases under ambient pressure at the temperature range of 0–1000 K. In the next step, we computed the phonon dispersion curves of six considered phases containing four stable configurations (*P*6/*mmm*-YB_2, $P12_1/c1$-Y_2B_5, *P*4/*mbm*-YB_4 and *Fm*–3 *m*-YB_{12}) and two low-enthalpy metastable phases (*Cmcm*-YB and *Pm*–3 *m*-YB_6), as presented in Fig. 2. It should be pointed out that our phonon calculations confirm the dynamical stabilities of six concerned yttrium borides with the evidence of the absence of any imaginary frequencies over the entire Brillouin zones. Moreover, we have also conducted AIMD simulations to evaluate the thermal stability of six concerned yttrium borides at the temperature of 300 K with the time step of 2 fs and supercells of 144, 81, 112, 160, 56 and 52 atoms for *Cmcm*-YB, *P*6/*mmm*-YB_2, $P12_1/c1$-Y_2B_5, *P*4/*mbm*-YB_4, *Pm*–3 *m*-YB_6, and *Fm*–3 *m*-YB_{12}, respectively, as depicted in Fig. S3. The computed consequences substantiate that all six yttrium borides keep stable at the temperature of 300 K.

3.2. Detailed crystalline structural characteristics

To look into the structural characters of six yttrium borides considered (*Cmcm*-YB, *P*6/*mmm*-YB_2, $P12_1/c1$-Y_2B_5, *P*4/*mbm*-YB_4, *Pm*–3 *m*-YB_6, and *Fm*–3 *m*-YB_{12}), we optimize their unit cell and draw the detailed structural diagrams in Fig. 3. Next, we probe into the detailed structural features according to the order of the increasing boron content. For the *Cmcm*-YB crystal, the unit cell contains four Y and four B atoms (see Fig. 3 (a)). In this crystalline structure, each Y atom is surrounded by six B atoms with two B atoms at a separation of 2.610 Å and four B atoms at a separation of 2.724 Å, forming a bottom regular triangular prism. The B atoms exhibit the zigzag arrangement along the *c* axis with the equal B–B bond length of 1.705 Å. In addition, the adjacent zigzag B chains are parallel to each other. These results indicate that the boron framework in the *Cmcm*-YB structure contains the zigzag B chains. Next, the hexagonal *P*6/*mmm*-YB_2 phase in the AlB_2-type structure (see Fig. 3(b)) contains the alternating B layers and Y layers within an intriguing B_6–Y–B_6 sandwiches stacking order along the *c* axis. It should be noted that each Y atom is located at the center of a regular hexagonal column with an equal Y–B bond distance of 2.710 Å and B atoms form parallel hexagonal planes with the equal adjacent B–B bond length of 1.903 Å. Thus, the boron network in the *P*6/*mmm*-YB_2 crystal consists of the planar hexagonal B rings. The newly predicted $P12_1/c1$-Y_2B_5 structure (Fig. 3(c)) belongs to the monoclinic crystal system and is composed of eight Y atoms and twenty B atoms. Y atoms take the Wyckoff 4e positions, (0.232, 0.193, 0.627) and (0.242, 0.815, 1.253), while B atoms occupy-five nonequivalent sites in this unit cell, the Wyckoff 4e (0.503, 0.674, 0.540), 4e (0.501, 0.089, 1.410), 4e (0.503, 0.038, 1.174), 4e (0.074, 0.990, 0.925), and 4e (0.686, 0.002, 1.041) positions. In the $P12_1/c1$-Y_2B_5 structure, one Y atom is surrounded by twelve B atoms with the Y–B separations varying from 2.613 to 2.993 Å and the B–Y–B angles varying between 33°and 157°. Furthermore, this structure also contains distorted B_6 octahedrons and seven-member B rings in one plane. Interestingly, the B_6 octahedron consists of three different rectangles with the equal B–B bond length of the reciprocal opposite sides. Six B–B bond lengths are 1.786, 1.791, 1.794, 1.797, 1.808 and 1.816 Å, respectively. In the seven-member B ring, two equal B–B bond lengths are 1.722 Å, two equal B–B bond lengths are 1.723 Å, one B–B bond length is 1.780 Å. In the meantime, another two different B–B bond lengths, 1.786 and 1.794 Å, overlap with two equatorial B–B bond lengths of the B_6 octahedrons. The consequences demonstrate that the boron framework for the $P12_1/c1$-Y_2B_5 structure is best described as distorted B_6 octahedrons and seven-member B rings. In the tetragonal *P*4/*mbm*-YB_4 polymorph (Fig. 3(d)), each Y atom is linked by 18 adjacent B atoms with four B atoms at a separation of 2.727 Å, four B atoms at a separation of 2.741 Å, four B atoms at a separation of 2.825 Å, four B atoms at a separation of 2.856 Å, and two B atoms at a separation of 3.069 Å. This crystal is also composed of slightly distorted B_6 octahedrons and seven-member B rings in a plane. In this B_6 octahedron, there exist two equal rectangular pyramids and each rectangular pyramid is composed of four identical isosceles triangles: eight lateral-edge B–B distances are 1.751 Å and four B–B distances in the basal surface are 1.811 Å. In the seven-member B ring, there exit four B–B distances of 1.718 Å, two B–B distances of 1.811 Å and one B–B distance of 1.746 Å. Simultaneously, the B–B distance of 1.811 Å is overlapping with the B–B distance in the basal surface of rectangular pyramid in B_6 octahedron. In consequence, the boron construction of the *P*4/*mbm*-YB_4 polycrystalline is constituted by slightly distorted B_6 octahedrons and planar seven-member B rings. For the cubic *Pm*–3 *m*-YB_6 configuration, as presented in Fig. 3(e), one Y atom possesses 24 adjacent B atoms with the equal Y–B distance of 3.010 Å. Moreover, this phase consists of two-dimensional eight-member B rings and regular B_6 octahedrons with the equal B–B distance of 1.745 Å. In the planar eight-member B rings, there are four B–B bond lengths of 1.631 Å and four B–B bond lengths of 1.745 Å, declaring a slightly distorted planar eight-member B ring. Hence, the boron configuration for the *Pm*–3 *m*-YB_6 structure can be characterized as slightly distorted planar eight-member B rings and regular B_6 octahedrons. In the cubic *Fm*–3 *m*-YB_{12} polymorph, one Y atom is located at the center of the particular B_{24} cage with all the equal Y-B distance of 2.786 Å (Fig. 3 (f)). Furthermore, the special B_{24} cage is constructed from eight planar hexagons and six standard squares. In a two-dimensional hexagon, there are three B–B bond distances of 1.789 Å and three B–B bond distances of 1.722 Å. Based on the rounded analyses of the

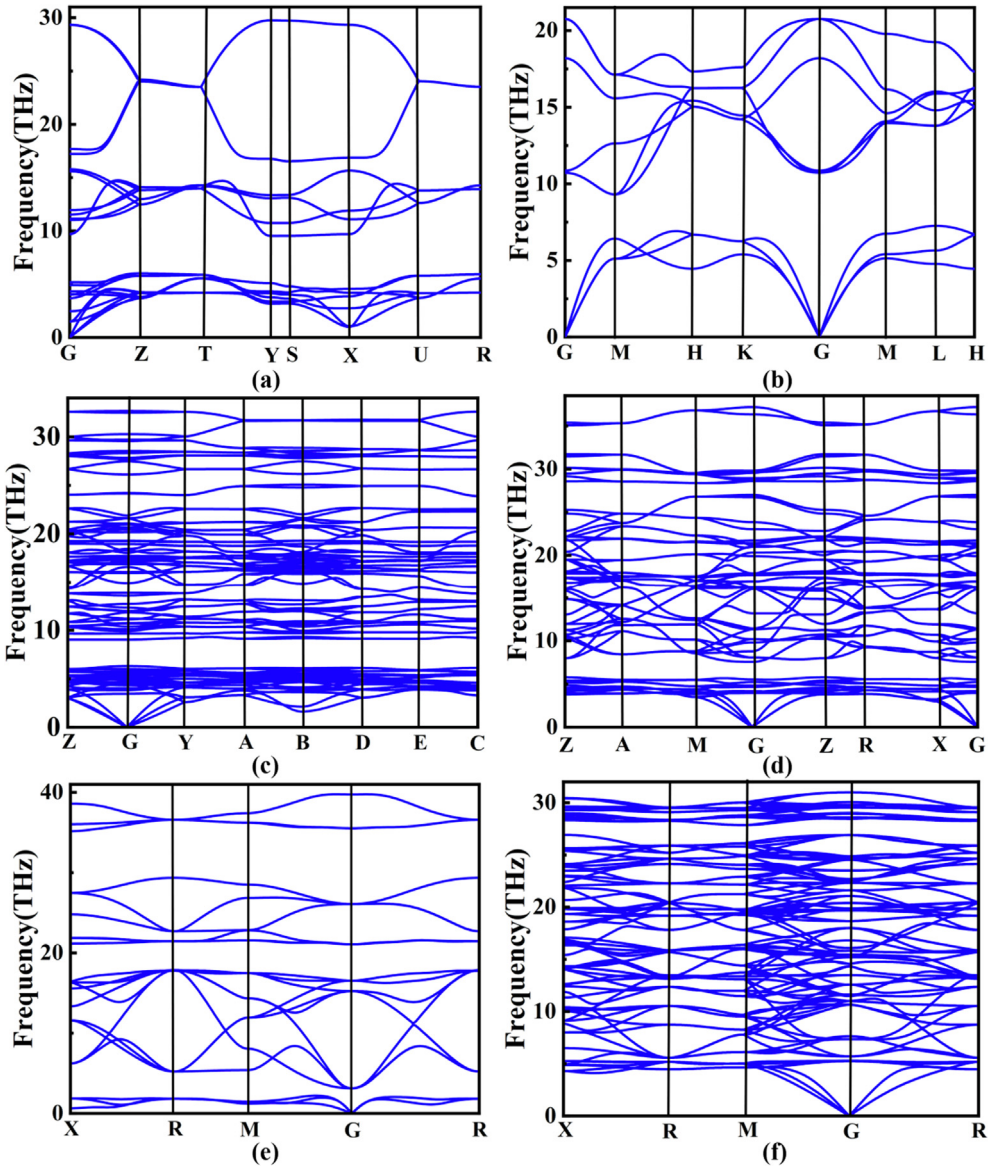

Fig. 2 Phonon dispersion curves of six considered Y–B compounds: (a) *Cmcm*–YB, (b) *P6/mmm*–YB_2, (c) *P*121/*c*1–Y_2B_5, (d) *P4/mbm*–YB_4, (e) *Pm*–3 *m*–YB_6 and (f) *Fm*–3 *m*–YB_{12}.

structural characters for six considered Y–B compounds, the B–B network of these six considered yttrium borides also undergoes a range of transformation with the increasing B concentration: zigzag B chains → planar hexagonal B rings → distorted B_6 octahedrons and planar seven-member B rings → slightly distorted B_6 octahedrons and planar seven-member B rings → regular B_6 octahedrons and planar eight-member B rings → B_{24} cages. The results above demonstrate that the boron framework for six considered Y–B compounds transform from quasi one-dimensional chain to two-dimensional B ring to a combination of two-dimensional B ring and three-dimensional B_6 octahedron to B_{24} cage as the B content increases, revealing the increasing dimension with the increasing B concentration in yttrium borides. Simultaneously, the Y–B distances in these six yttrium borides vary from 2.610 to 3.010 Å, which are larger than the sum (2.44 Å) of the covalent radii of Y (r = 1.62 Å) and B (r = 0.82 Å), revealing the inexistence of Y–B covalent bonding interaction. Moreover, the range of B–B bond lengths (1.631–1.903 Å) of the boron network is comparable to that of α-B (1.669–2.003 Å) (Li et al., 1992) and γ-B (1.661–1.903 Å) (Oganov et al., 2009); implying a B–B covalent network in six studied yttrium borides. Overall, the boron network in six considered Y–B compounds should have B–B covalent bond.

3.3. Electronic properties and bonding features

The intriguing structural features for six focused yttrium borides (*Cmcm*-YB, *P6/mmm*-YB_2, *P*$12_1/c1$-Y_2B_5, *P4/mbm*-YB_4, *Pm*–3 *m*-YB_6, and *Fm*–3 *m*-YB_{12}) further arouse our curiosity of exploring their electronic properties and bonding features. Following, we computed the band structures and density of states with the corresponding figures depicted in Fig. 4. Obviously, all the Y–B compounds present the metallic characters

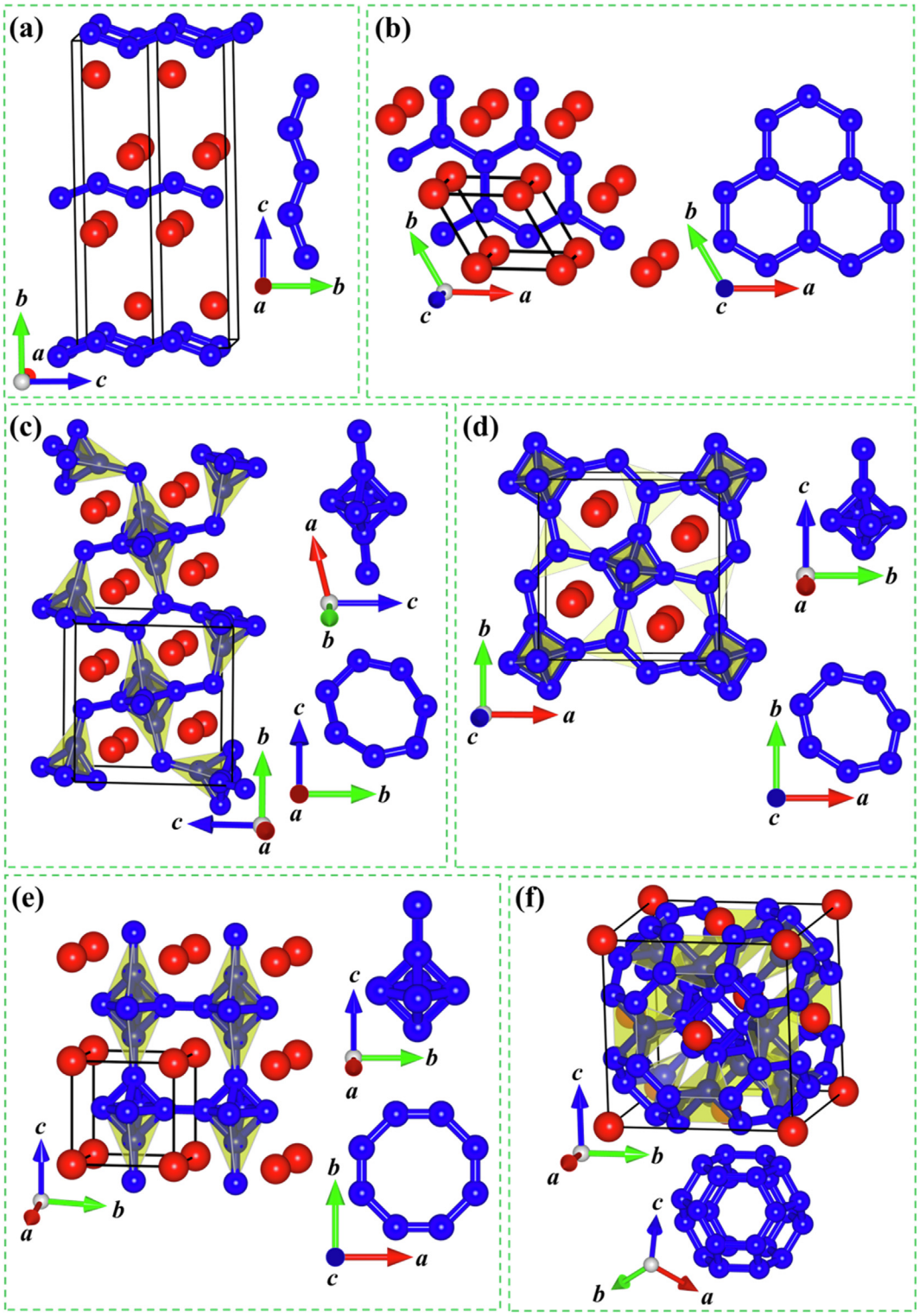

Fig. 3 Crystal structures of six considered Y–B compounds: (a) *Cmcm*–YB, (b) *P*6/*mmm*–YB_2, (c) *P*121/*c*1–Y_2B_5, (d) *P*4/*mbm*–YB_4, (e) *Pm*–3 *m*–YB_6 and (f) *Fm*–3 *m*–YB_{12}. The red and blue spheres represent Y and B atoms, respectively.

with the evidence of some energy bands crossing the Fermi level (EF). In addition, the total density of states (TDOS) near the Fermi level is largely contributed by the Y–4*d* and B–2*p* states. The unremarkable hybridization phenomenon between the Y–4*d* and B–2*p* states near the Fermi level reflects the relatively weak interaction between Y and B atoms. Meanwhile, the occupied electronic states in the valence region are dominated by B–2 *s* and B–2*p* states, while partial contributions from the Y atoms is trivial can be neglected. This indicates that the valence electrons of Y are mostly transferred to the B atoms and that the Y–B interaction in six considered Y–B compounds possesses the ionic character. To further explore

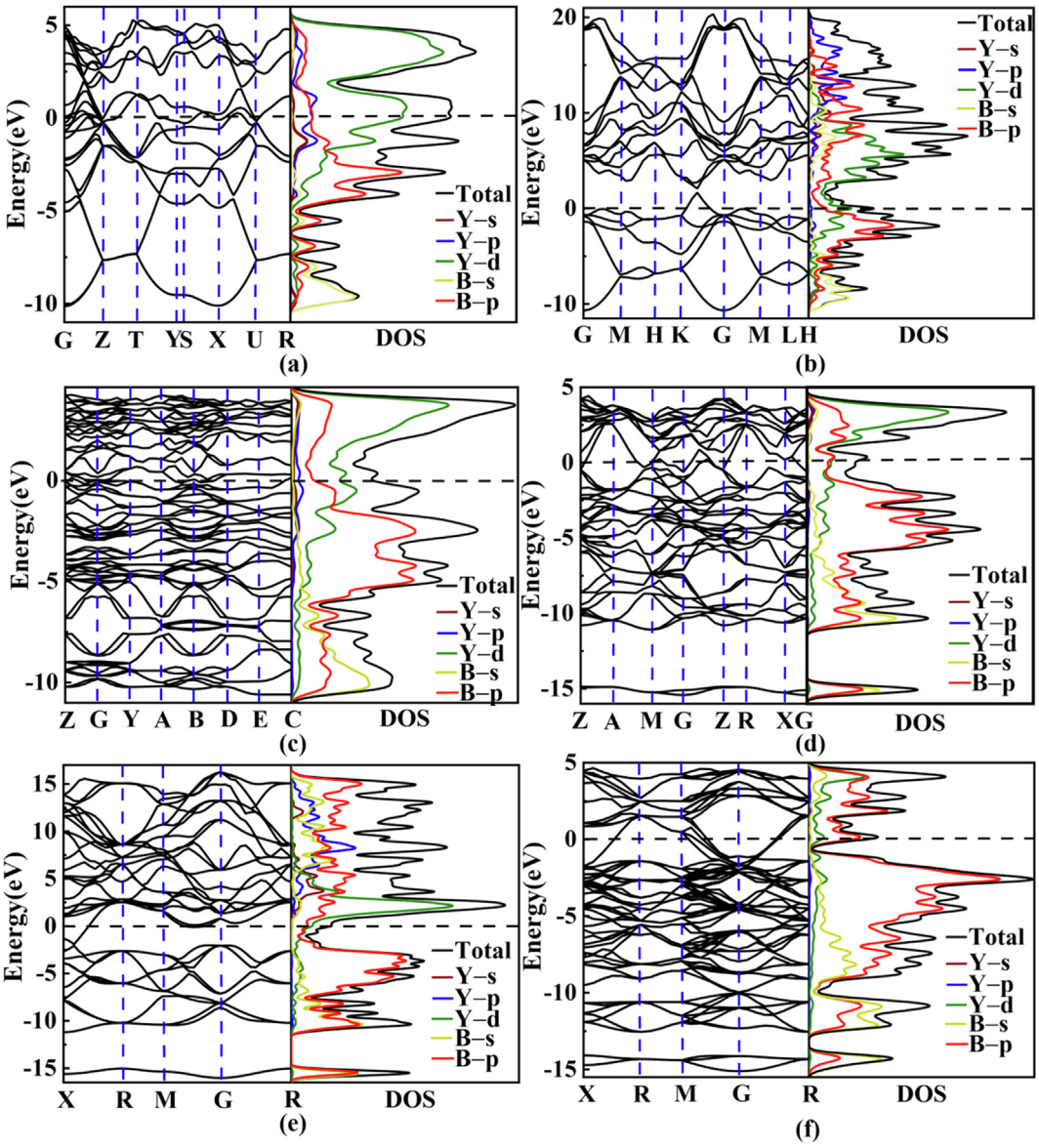

Fig. 4 Band structures and density of states for six considered Y–B compounds: (a) *Cmcm*–YB, (b) *P*6/*mmm*–YB_2, (c) *P*121/*c*1–Y_2B_5, (d) *P*4/*mbm*–YB_4, (e) *Pm*–3 *m*–YB_6 and (f) *Fm*–3 *m*–YB_{12}.

the bonding nature of six studied yttrium borides, we computed their electron localization function (ELF) (Becke and Edgecombe, 1990; Savin et al., 1992), as plotted in Fig. 5. From Fig. 5, it is clearly seen that high electron localization exists in the region between B atoms, declaring the strong B–B covalent bonding within the boron framework in six considered yttrium borides. In comparison, ionic bonding is formed between Y and B atoms, which is in consistent with the aforementioned DOS analysis and corroborated by the further Bader partial charge analysis (see Table 1) (Bader, 1994), which stems from large amounts of charge transferred from Y to the B–B covalent network. To further clarify the relative bond strength between Y–B and B–B covalent framework for six concerned yttrium borides at ambient pressure, we have calculated the crystal orbital Hamilton population (COHP) and integral crystal orbital Hamilton population (ICOHP) as executed in the LOBSTER package (Dronskowski and Bloechl, 1993; Maintz et al., 2016); as displayed in Fig. 6. The predicted ICOHPs of B–B pair is much larger than that of Y–B pair, demonstrating that the B–B interaction is much stronger than that of Y–B. In short, we can speculate that the chemical bonding in six concerned yttrium borides comprises of positively charged metal Y cation and negatively charged B–B covalent framework. This bonding configuration can also be found in other metal borides, such as MgB_2 (Tateishi et al., 2019), YB_6 (Wang et al., 2018) and YB_{12} (Czopnik et al., 2005).

3.4. Mechanical properties and Vickers hardness

Based on the robust thermal and dynamical stabilities under atmospheric pressure, as well as particular structural characters and strong covalent B–B frames, it is necessary to gain insight into the mechanical properties of six considered yttrium

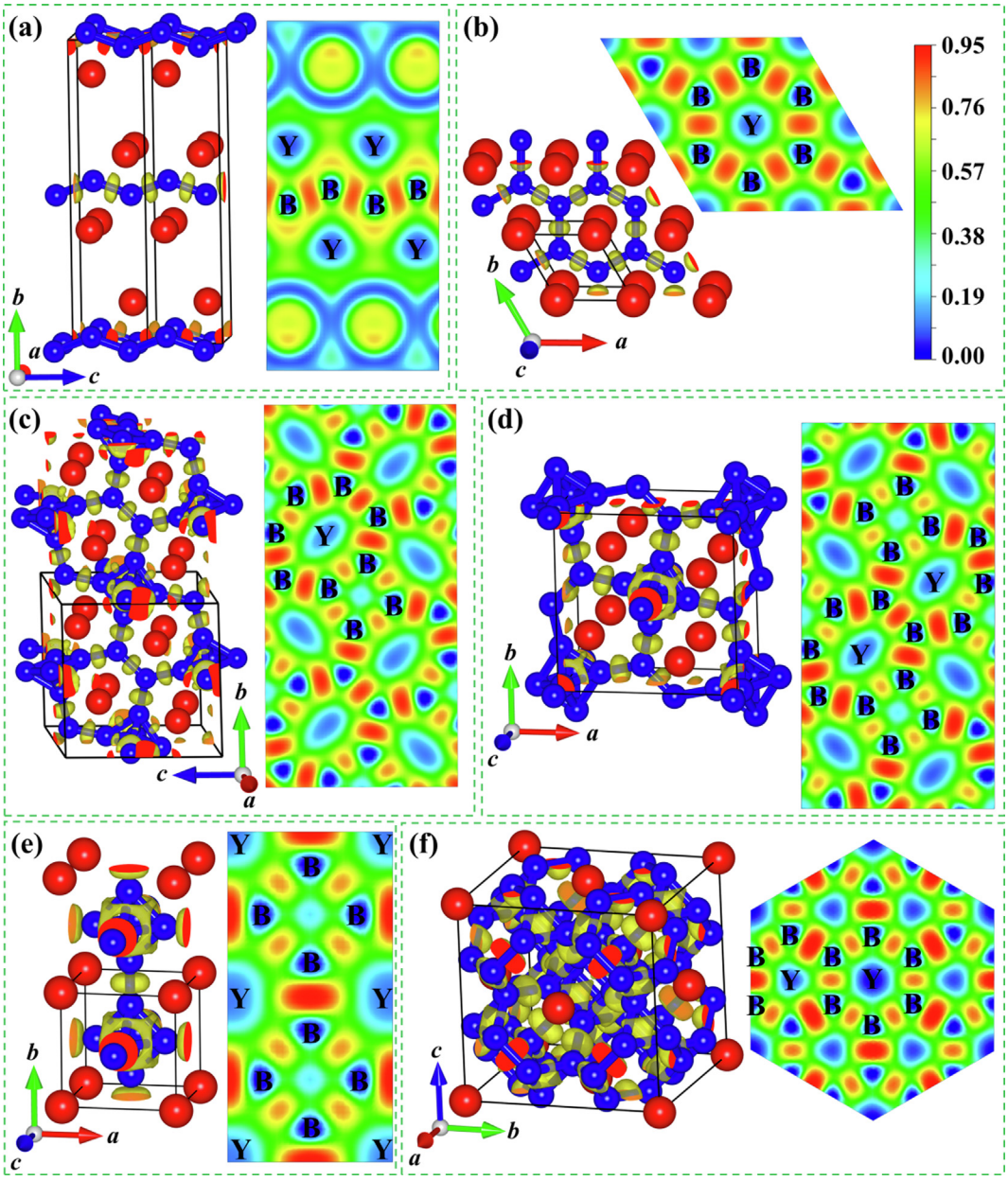

Fig. 5 Three-dimensional electron localization functions (ELFs) with an isosurface 0.77 and two-dimensional ELFs on the corresponding planes for six considered Y–B compounds. (a) *Cmcm*–YB (1 0 0), (b) *P*6/*mmm*–YB_2 (0 0 1), (c) $P12_1/c1$–Y_2B_5 (1 0 0), (d) *P*4/*mbm*–YB_4 (0 0 1), (e) *Pm*–3 *m*–YB_6 (0 0 1) and (f) *Fm*–3 *m*–YB_{12} (1 1 1).

borides (*Cmcm*-YB, *P*6/*mmm*-YB_2, $P12_1/c1$-Y_2B_5, *P*4/*mbm*-YB_4, *Pm*–3 *m*-YB_6, and *Fm*–3 *m*-YB_{12}) which are important parameters for assessment as promising near-superhard or hard materials for engineering applications. Thus, we computed their elastic constants by employing the strain–stress method (Lu et al., 2010), as displayed in Table 2. Furthermore, the elastic constants can also be used to verify the mechanical stabilities of the materials. It is found from Table 2 that all the six considered yttrium borides meet their corresponding mechanical stability standard (Wu et al., 2007), confirming their mechanical stabilities. Based on the calculated elastic constants, the bulk modulus (B), shear modulus (G), Young's modulus (E), B/G, Poisson's ratio (v) and Debye temperature (Θ) for six considered Y–B compounds were further estimated within the Voigt–Reuss–Hill method (Connétable and Thomas, 2009), as presented in Table 2. Beyond the present computed consequences, Table 2 also lists the previous theoretical results of *P*4/*mbm*–YB_4 (Fu et al., 2014) and *Pm*–3 *m*–YB_6 (Romero et al., 2019) for comparison. It can clearly be found that the calculated results in present work are consistent with the reported theoretical consequences (Fu et al., 2014; Romero et al., 2019); confirming the reliability of the present calculations. The predicted values of C_{11}; C_{22}, and C_{33} for six considered crystals are considerable, illustrating that they possess very strong incompressibility along a, b, and c axis, respectively. C_{44} is another significant parameter which is indirectly related to the indentation hardness of a material. As presented in Table 2, these four compounds studied (*P*6/*mmm*-YB_2, $P12_1/c1$-Y_2B_5, *P*4/*mbm*-YB_4, and *Fm*–3 *m*-YB_{12}) exhibit relatively high C_{44} values (> 100 GPa), uncover-

Table 1 Calculated Bader charges of Y and B atoms in six considered Y–B compounds. δ represents the amount of charge transferred from Y atom to B atom.

Composition	Space group	Atom	Change value (e)	δ (e)
YB	*Cmcm*	Y	9.89	1.11
		B	4.11	–1.11
YB_2	*P6/mmm*	Y	9.45	1.55
		B	3.78	–0.78
Y_2B_5	$P12_1/c1$	Y	9.46	1.54
		B	3.62	–0.62
YB_4	*P4/mbm*	Y	9.29	1.71
		B	3.43	–0.43
YB_6	*Pm*-3 *m*	Y	9.13	1.87
		B	3.31	–0.31
YB_{12}	*Fm*-3 *m*	Y	9.22	1.78
		B	3.15	–0.15

ing a strong strength of resisting the shear deformation. On the contrary, the remainder two compounds considered, *Cmcm*-YB and *Pm*–3 *m*-YB_6, have relatively low C_{44} values (< 100 GPa), reflecting the weak shear strength.

As is generally known, the bulk modulus B of a material is an index of the ability to resist uniform compression. The higher bulk modulus B of a material corresponds to the stronger ability in resisting uniform compression. From Table 2, the computed bulk modulus varies from 78 to 222 GPa. Among these six compounds studied, *Fm*–3 *m*–YB_{12} has the highest bulk modulus of 222 GPa, which is slightly less than that of common hard materials such as α-Ti_3B_4 (234 GPa) (Zhao et al., 2018) and β-Ti_3B_4 (235 GPa) (Zhao et al., 2018); *Cmcm*-HfB_4 (239 GPa) (Chang et al., 2018); *Cmcm*-ZrB_4 (234 GPa) (Chang et al., 2018); Fe_3C (226.8 GPa) (Jang et al., 2009) and TiC (242 GPa) (Gilman and Roberts, 1961). To our knowledge, compared with bulk modulus, the shear modulus and Young modulus of a material exhibit stronger correlation with the hardness (Fulcher et al., 2012). As presented in Table 2, the *Fm*–3 *m*-YB_{12} phase possesses the largest shear modulus (195 GPa) and the highest Young modulus (453 GPa), revealing that this polycrystalline is expected to be the hardest compound among all the yttrium borides. In addition,

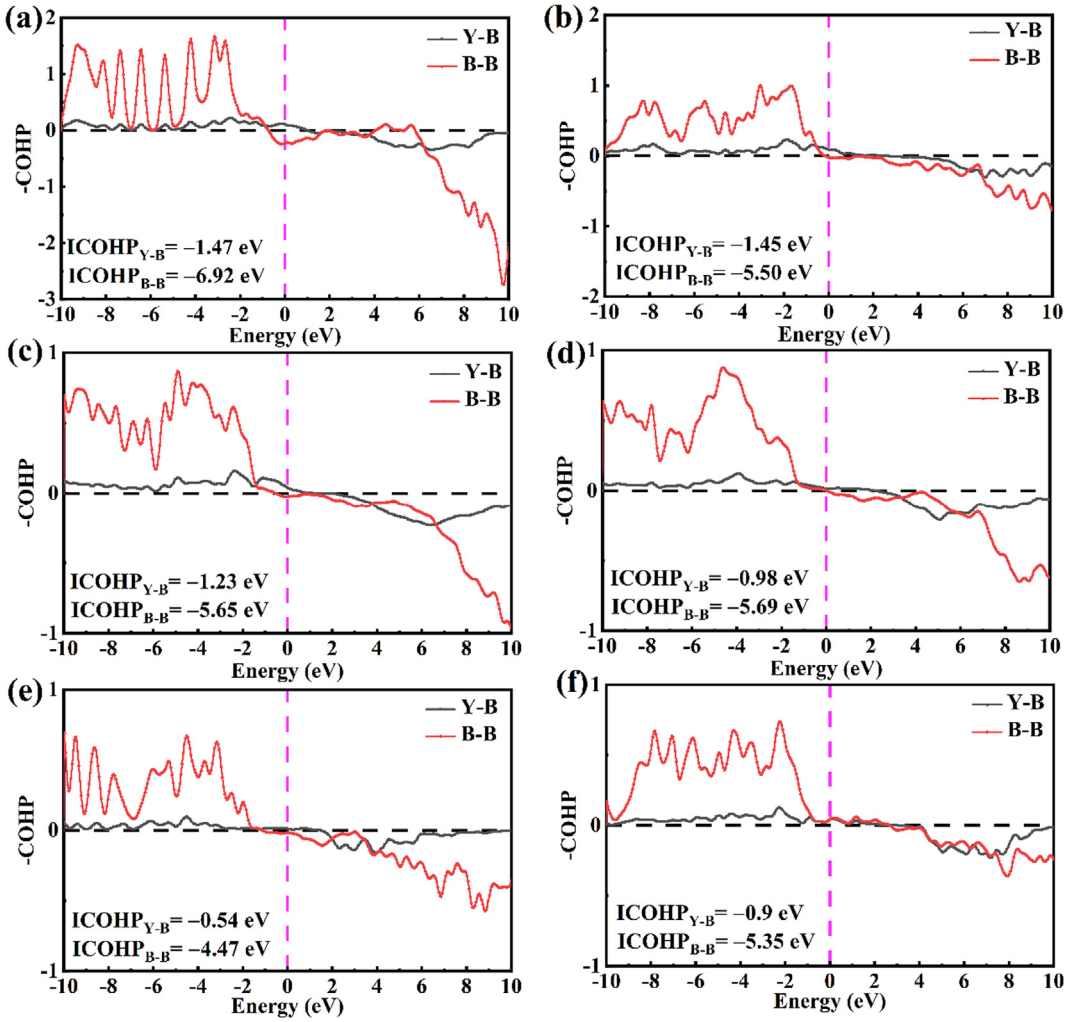

Fig. 6 The crystal orbital Hamilton population (COHP) curves for (a) *Cmcm*–YB, (b) *P6/mmm*–YB_2, (c) $P121/c1$–Y_2B_5, (d) *P4/mbm*–YB_4, (e) *Pm*–3 *m*–YB_6 and (f) *Fm*–3 *m*–YB_{12}. The dotted vertical line at 0 eV denotes Fermi energy level.

Table 2 Calculated elastic constants C_{ij} (GPa), bulk modulus B (GPa), shear modulus G (GPa), Young's modulus E (GPa), B/G, Poisson's Ratio v, Debye temperature Θ (K), and Vickers hardness H_v (GPa) of six considered yttrium borides.

	Cmcm- YB	*P*6/*mmm*-YB_2	*P*$12_1/c1$-Y_2B_5	*P*4/*mbm*-YB_4	*P*4/*mbm*-YB_4	*Pm*-3 *m* -YB_6	*Pm*-3 *m* -YB_6	*Fm*-3 *m* -YB_{12}
C_{11}	158	376	319	436	454[a]	447	455[b]	411
C_{12}	59	57	37	78	80[a]	36	38[b]	128
C_{13}	10	91	38	46	33[a]			
C_{15}			–34					
C_{22}	101		327					
C_{23}	29		66					
C_{25}			12					
C_{33}	277	339	305	431	442[a]			
C_{35}			9					
C_{44}	35	163	122	107	108[a]	31	21[b]	243
C_{46}			9					
C_{55}	48		92					
C_{66}	54		70	128	132[a]			
B	78	173	136	182	182[a]	173	176[b]	222
G	51	151	106	139	144[a]	74	64[b]	195
E	127	350	253	333	342[a]	194	171[b]	453
B/G	1.52	1.15	1.28	1.31		2.35		1.14
v	0.23	0.16	0.19	0.19	0.18[a]	0.31	0.34[b]	0.16
Θ	400	743	660	818	874[a]	648		1166
H_v	9.31	27.49	18.83	22.29		7.34	5.49[b]	33.16

[a] Reference Fu et al., 2014.
[b] Reference Romero et al., 2019.

another important parameter, B/G, is normally used to evaluate the ductility of a material. The high B/G ratio of a material (>1.75) can be classified into a ductile material while the low B/G ratio of a material (<1.75) corresponds to a brittle material (Pugh, 1954). In the view of classification rule, the *Pm*–3 *m*-YB_6 compound possesses a B/G ratio of 2.35, demonstrating the ductile feature, while the other five crystals have B/G ratio $<$ 1.75, suggesting brittle behaviors. The Poisson's ratio v is a critical target to estimate the degree of the directionality for the covalent bonds. As displayed in Table 2, the fact that the Poisson's ratio v for six focused yttrium borides (except for YB and YB_6) are relatively low (<0.20) confirms their strong covalent bonding. Mechanical properties (in particular, hardness of a solid) are connected with thermodynamic parameters, including Debye temperature, specific heat, thermal expansion, and melting point (Abrahams and Hsu, 1975). In this concept, the Debye temperature (Θ) is one of the fundamental parameters for the characterization of materials and the hardness of a solid. Therefore, the Debye temperature (Θ) could be estimated on the account of the elastic constants at low temperature (Ravindran et al., 1998; Anderson, 1963). In Table 2, the derived Debye temperature (Θ) in YB_{12} can reach 1166 K, which is higher than those of ReB_2 (755.5 K) (Aydin and Simsek, 2009), FeB_4 (1089 K) (Zhang et al., 2013), TcB_4 (1050 K) (Zhao and Xu, 2012), ReB_4 (824 K) (Zhao and Xu, 2012). The Debye temperature value of YB_{12} is situated between that of superhard material ReB_2 (755.5 K) and diamond (2230 K), indicating that YB_{12} should be harder than these superhard materials mentioned above (except for diamond).

In the view of the large shear modulus G, Young modulus E and Debye temperature Θ coupled with the small values for the B/G ratio and Poisson's ratio ν as tabulated in Table 2, the *Fm*–3 *m*–YB_{12} crystal may be expected to have high hardness among the Y-B compounds. We now further explore the Vickers hardness for six considered yttrium borides (*Cmcm*-YB, *P*6/*mmm*-YB_2, *P*$12_1/c1$-Y_2B_5, *P*4/*mbm*-YB_4, *Pm*–3 *m*-YB_6, and *Fm*–3 *m*-YB_{12}) with the microscopic hardness model proposed by Tian *et al* (Tian et al., 2012). The Vickers hardness of complex crystals can be estimated by the following formula:

$$H_v = 0.92K^{1.137}G^{0.708} \quad (3)$$

Herein, $K = G/B$, B and G represent the bulk modulus and shear modulus of the crystal. The calculated consequences for six concerning yttrium borides are summarized in Table 2. The fact that the present hardness values of 22.29 and 7.34 GPa for the *P*4/*mbm*-YB_4 and *Pm*–3 *m*-YB_6 crystalline structures are respectively consistent with the experimental value of YB_4 (27.4 GPa) (Zaykoski et al., 2011) and the previous theoretical result for YB_6 (5.49 GPa) (Romero et al., 2019) confirms the reliability of our calculations. The novel *P*$12_1/c1$-Y_2B_5 structure possesses a hardness value of 18.83 GPa, which approaches that of the famous hard material Al_2O_3 (20 GPa) (Andrievski, 2001), revealing the hard character. More importantly, the Vickers hardness value for YB_{12} can reach 33.16 GPa, which is higher than those of WB_4 (31.8 GPa) (Gu et al., 2008), WC (30 GPa) (Haines et al., 2001); BP (33 GPa) (Andrievski, 2001); β-Si_3N_4 (30 GPa) (Andrievski, 2001), and TiC (32 GPa) (Guo et al., 2008), close to the lower limit of superhard materials (40 GPa). The analysis on the hardness of the YB_{12} compound suggests this crystal has the ultra-incompressible nature and can be regarded as a promising superhard material. Compared with the other four considered yttrium borides (*P*6/*mmm*-YB_2, *P*$12_1/c1$-Y_2B_5, *P*4/*mbm*-YB_4, and *Fm*–3 *m*-YB_{12}) with higher hardness values (>18 GPa), the *Cmcm*-YB and *Pm*–3 *m*-YB_6 configurations possess the lower hardness values of 9.31 and 7.34 GPa. In general, the

origin of differences in hardness is related not only to the strengths of B–B covalent bonds but also to the configuration of the boron framework. The *Cmcm*-YB phase with low hardness value can be ascribed to the zigzag B chain without the formation of the complex boron network, such as planar and three-dimensional covalent framework. Contrary to the *Cmcm*-YB phase, the *Pm*–3 *m*-YB_6 crystal accompanied with the low hardness value should be attributed to the intrinsic ductile and soft character, which stems from the weak banana bond within the B_6 octahedron (Zhou et al., 2015). Thus, the strong covalent B–B bond as well as the complex B–B covalent network are responsible for the high hardness, high shear modulus, high Young's modulus as well as low Poisson's ratio for four considered yttrium borides (*P*6/*mmm*-YB_2, *P*12$_1$/*c*1-Y_2B_5, *P*4/*mbm*-YB_4, and *Fm*–3 *m*-YB_{12}).

4. Conclusions

To sum up, the exploration of the stable and metastable structures of boron-rich yttrium borides is a widely concerned subject in the fundamentally and practically functional materials because of their uniquely mechanical, superconductive and thermoelectric properties. In the present work, based on the CALYPSO prediction method coupled with the first-principles calculation, we conducted a systematical investigation on the stable and metastable configurations in the Y–B binary system, especially on the boron-rich side. In addition to four experimentally known phases, *P*6/*mmm*–YB_2, *P*4/*mbm*–YB_4, *Pm*–3 *m*–YB_6 and *Fm*–3 *m*–YB_{12}, we uncover a new stable Y_2B_5 compound with the monoclinic *P*12$_1$/*c*1 phase. In particular, the *P*12$_1$/*c*1–Y_2B_5 phase is a solely stable phase within an unprecedentedly fractional stoichiometry in the Y–B binary system. Structurally, the *P*12$_1$/*c*1-Y_2B_5 crystalline contains the distorted B_6 octahedron and seven-member B ring. Moreover, the computed formation enthalpy, elastic constants, and phonon dispersion curves verify that the *P*12$_1$/*c*1–Y_2B_5 structure is energetically, mechanically, and dynamically stable, respectively. Further analysis on the bond length, density of states, electron localization function, Bader charge and crystal orbital Hamilton population (COHP) reveals that the bonding pattern in *P*12$_1$/*c*1–Y_2B_5 can be deemed as a combination of positively charged metal Y cation and negatively charged B–B covalent framework. Surprisingly, as the B content increases, the B–B bonding form in six concerned yttrium borides undergoes an increasing dimension, quasi one-dimensional chain → two-dimensional B ring → a combination of two-dimensional B ring and three-dimensional B_6 octahedron → three-dimensional B_{24} cage. Based on a microscopic hardness model, the Vickers hardness value of *P*12$_1$/*c*1–Y_2B_5 is 18.83 GPa, indicating an incompressible and hard material. More interestingly, *Fm*-3 *m*-YB_{12} can be classified into an ultra-incompressible material with the significant hardness of 33.16 GPa. The high hardness for both phases can be attributed to the strong covalent B–B bond as well as the complex B–B covalent network. We anticipate that our work can motivate future experimental and theoretical investigations on the newly predicted boron-rich yttrium borides.

Declaration of Competing Interest

The authors declare that they have no known competing financial interests or personal relationships that could have appeared to influence the work reported in this paper.

Acknowledgements

This work was supported by the National Natural Science Foundation of China (No. 11804031, 11904297, 11904032 and 11747139), the Scientific Research Project of Education Department of Hubei Province (No. Q20191301), Talent and High Level Thesis Development Fund of Department of Physics and Optoelectronic Engineering of Yangtze University (C. Z. Z.), and Yangtze University Innovation and Entrepreneurship Project (No. 2019364).

Appendix A. Supplementary material

Supplementary data to this article can be found online at https://doi.org/10.1016/j.arabjc.2023.104546.

References

Abrahams, S.C., Hsu, F.S.L., 1975. Debye temperatures and cohesive properties. J. Chem. Phys. 63 (3), 1162–1165.
Anderson, O.L., 1963. A simplified method for calculating the Debye temperature from elastic constants. J Phys. Chem. Solids 24 (7), 909–917.
Andrievski, R.A., 2001. Superhard materials based on nanostructured high-melting point compounds: achievements and perspectives. Int. J. Refract. Met. Hard Mater. 19 (4–6), 447–452.
Aydin, S., Simsek, M., 2009. First-principles calculations of MnB_2, TcB_2, and ReB_2 within the ReB_2-type structure. Phys. Rev. B 80, (13) 134107.
R.F. Bader, Atoms in Molecules: A Quantum Theory (1994).
Becke, A.D., Edgecombe, K.E., 1990. A simple measure of electron localization in atomic and molecular systems. J. Chem. Phys. 92, 5397–5403.
Chang, J., Zhou, X., Liu, K., Ge, N., 2018. Structural, elastic, mechanical and thermodynamic properties of HfB_4 under high pressure. R. Soc. Open Sci. 5, (7) 180701.
Chen, B., Conway, L.J., Sun, W., Kuang, X., Lu, C., Hermann, A., 2021. Phase stability and superconductivity of lead hydrides at high pressure. Phys. Rev. B 103, 035131.
Chung, H.Y., Weinberger, M.B., Levine, J.B., Kavner, A., Yang, J.M., Tolbert, S.H., Kaner, R.B., 2007. Synthesis of ultra-incompressible superhard rhenium diboride at ambient pressure. Science 316, 436–439.
Connétable, D., Thomas, O., 2009. First-principles study of the structural, electronic, vibrational, and elastic properties of orthorhombic NiSi. Phys. Rev. B 79, 094101.
Cumberland, R.W., Weinberger, M.B., Gilman, J.J., Clark, S.M., Tolbert, S.H., Kaner, R.B., 2005. Osmium diboride, an ultra-incompressible, hard material. J. Am. Chem. Soc. 127, 7264–7265.
Czopnik, A., Shitsevalova, N., Pluzhnikov, V., Krivchikov, A., Paderno, Y., Onuki, Y., 2005. Low-temperature thermal properties of yttrium and lutetium dodecaborides. J. Phys.: Condens. Matter 17, 5971–5985.
Decker, B.F., Kasper, J.S., 1959. The crystal structure of a simple rhombohedral form of boron. Acta Crystallogr. 12, 503–506.
Ding, L.P., Tiandong, Y.H., Shao, P., Tang, Y., Zhao, Z.L., Lu, H., 2021. Crystal structures, phase stabilities, electronic properties, and hardness of yttrium borides: new insight from first-principles calculations. J. Phys. Chem. Lett. 12, 5423–5429.
Dronskowski, R., Bloechl, P.E., 1993. Crystal orbital Hamilton populations (COHP): energy-resolved visualization of chemical bonding in solids based on density-functional calculations. J. Chem. Phys. 97, 8617–8624.
Feng, J., Hennig, R.G., Ashcroft, N.W., Hoffmann, R., 2008. Emergent reduction of electronic state dimensionality in dense ordered Li-Be alloys. Nature 451, 445–448.
Fu, Y.Y., Li, Y.W., Huang, H.M., 2014. Elastic and dynamical properties of YB_4: first-principles study. Chin. Phys. Lett. 31, 116201.

Fulcher, B.D., Cui, X.Y., Delley, B., Stampfl, C., 2012. Hardness analysis of cubic metal mononitrides from first principles. Phys. Rev. B 85, 184106.

G. Ghosh, A.van de Walle, M. Asta, First-principles calculations of the structural and thermodynamic properties of bcc, fcc and hcp solid solutions in the Al–TM (TM = Ti, Zr and Hf) systems: a comparison of cluster expansion and supercell methods, Acta Mater. 56 (2008) 3202–3221.

Gilman, J.J., Roberts, B.W., 1961. Elastic constants of TiC and TiB_2. J. Appl. Phys. 32, 1405.

Gou, H., Dubrovinskaia, N., Bykova, E., Tsirlin, A.A., Kasinathan, D., Schnelle, W., Richter, A., Merlini, M., Hanfland, M., Abakumov, A.M., Batuk, D., Tendeloo, G.V., Nakajima, Y., Kolmogorov, A.N., Dubrovinsky, L., 2013. Discovery of a superhard iron tetraboride superconductor. Phys. Rev. Lett. 111, 157002.

Gou, H., Tsirlin, A.A., Bykova, E., Abakumov, A.M., Tendeloo, G. V., Richter, A., Ovsyannikov, S.V., Kurnosov, A.V., Trots, D.M., Konôpková, Z., Liermann, H.P., Dubrovinsky, L., Dubrovinskaia, N., 2014. Peierls distortion, magnetism, and high hardness of manganese tetraboride. Phys. Rev. B 89, 064108.

Q. Gu, Günter Krauss, W. Steurer, Transition metal borides: superhard versus ultra-incompressible, Adv. Mater. 20 (2008) 3620–3626.

Gu, C., Liang, Y., Zhou, X., Chen, J., Ma, D., Qin, J., Zhang, W., Zhang, Q., Daemen, L.L., Zhao, Y., Wang, S., 2021. Crystal structures and formation mechanisms of boron-rich tungsten borides. Phys. Rev. B 104, 014110.

Günster, J., Kawanowa, H., Tanaka, T., Souda, R., 1998. An investigation of the YB_{66} (100) surface. Surf. Sci. 419, 38–47.

Guo, X., Li, L., Liu, Z., Yu, D., He, J., Liu, R., Xu, B., Tian, Y., Wang, H.T., 2008. Hardness of covalent compounds: roles of metallic component and valence electrons. J. Appl. Phys. 104, 023503.

Haines, J., Léger, J.M., Bocquillon, G., 2001. Synthesis and design of superhard materials. Annu. Rev. Mater. Res. 31, 1–23.

Higashi, I., Kobayashi, K., Tanaka, T., Ishizawa, Y., 1997. Structure refinement of YB_{62} and YB_{56} of the YB_{66}-type structure. J. Solid State Chem. 133, 16–20.

Hill, R., 1952. The elastic behavior of a crystalline aggregate. Proc. Phys. Soc. London, Sect. A 65, 349.

Hossain, M.A., Tanaka, I., Tanaka, T., Khan, A.U., Mori, T., 2015. YB_{48} the metal rich boundary of YB_{66}; crystal growth and thermoelectric properties. J. Phys. Chem. Solids 87, 221–227.

Jäger, B., Paluch, S., Wolf, W., Herzig, P., Zogał, O.J., Shitsevalova, N., Paderno, Y., 2004. Characterization of the electronic properties of YB_4 and YB_6 using ^{11}B NMR and first-principles calculations. J. Alloy. Compd. 383, 232–238.

Jang, J.H., Kim, I.G., Bhadeshia, H.K.D.H., 2009. Substitutional solution of silicon in cementite: a first-principles study. Comput. Mater. Sci. 44, 1319–1326.

Y.Y. Jin, J.Q. Zhang, S. Ling, Y.Q. Wang, S. Li, F.G. Kuang, Z.Y. Wu, C.Z. Zhang, Pressure-induced novel structure with graphene-like boron-layer in titanium monoboride, Chin. Phys. B 10.1088/1674-1056/ac9222.

Jothi, P.R., Yubuta, K., Fokwa, B.P.T., 2018. A simple, general synthetic route toward nanoscale transition metal borides. Adv. Mater. 30, 1704181.

Kresse, G., Furthmüller, J., 1996. Efficient iterative schemes for ab initio total-energy calculations using a plane-wave basis set. Phys. Rev. B 54, 11169–11186.

Kresse, G., Joubert, D., 1999. From ultrasoft pseudopotentials to the projector augmented-wave method. Phys. Rev. B 59, 1758–1775.

Latini, A., Rau, J.V., Teghil, R., Generosi, A., Alberini, V.R., 2010. Superhard properties of rhodium and iridium boride films. ACS Appl. Mater. Interfaces 2, 581–587.

Levine, J.B., Tolbert, S.H., Kaner, R.B., 2009. Advancements in the search for superhard ultra-incompressible metal borides. Adv. Funct. Mater. 19, 3519–3533.

Li, D., Xu, Y.N., Ching, W.Y., 1992. Electronic structures, total energies, and optical properties of α-rhombohedral B_{12} and α-tetragonal B_{50} crystals. Phys. Rev. B 45, 5895–5905.

Li, P., Zhou, R., Zeng, X.C., 2015. Computational analysis of stable hard structures in the Ti–B system. ACS Appl. Mater. Interfaces 7, 15607–15617.

Liang, H., Peng, F., Guan, S., Tan, L., Chen, H., Lei, L., He, D., Lu, C., 2019. Abnormal physical behaviors of hafnium diboride under high pressure. Appl. Phys. Lett. 115, 231903.

Liao, P.K., Spear, K.E., 1995. The B–Y(boron–yttrium) system. J. Phase Equilib. 16 (6), 521–524.

Lortz, R., Wang, Y., Tutsch, U., Abe, S., Meingast, C., Popovich, P., Knafo, W., Shitsevalova, N., Paderno, Y.B., Junod, A., 2006. Superconductivity mediated by a soft phonon mode: specific heat, resistivity, thermal expansion, and magnetization of YB_6. Phys. Rev. B 73, 024512.

Lu, C., Kuang, X.Y., Wang, S.J., Zhao, Y.R., Tan, X.M., 2010. Theoretical investigation on the high-pressure structural transition and thermodynamic properties of cadmium oxide. Europhys. Lett. 91, 16002.

Lu, C., Gong, W., Li, Q., Chen, C., 2020. Elucidating stress-strain relations of ZrB_{12} from first-principles studies. J. Phys. Chem. Lett. 11, 9165–9170.

Lv, J., Wang, Y., Zhu, L., Ma, Y., 2011. Predicted novel high-pressure phases of lithium. Phys. Rev. Lett. 106, 015503.

Ma, T., Li, H., Zheng, X., Wang, S., Wang, X., Zhao, H., Han, S., Liu, J., Zhang, R., Zhu, P., Long, Y., Cheng, J., Ma, Y., Zhao, Y., Jin, C., Yu, X., 2017. Ultrastrong boron frameworks in ZrB_{12}: a highway for electron conducting. Adv. Mater. 29, 1604003.

Maintz, S., Deringer, V.L., Tchougréeff, A.L., Dronskowski, R., 2016. LOBSTER: A tool to extract chemical bonding from plane-wave based DFT. J. Comput. Chem. 37, 1030–1035.

Martyna, G.J., Klein, M.L., Tuckerman, M., 1992. Nosé-Hoover chains: The canonical ensemble via continuous dynamics. J. Chem. Phys. 97, 2635–2643.

Mohammadi, R., Lech, A.T., Xie, M., Weaver, B.E., Yeung, M.T., Tolbert, S.H., Kaner, R.B., 2011. Tungsten tetraboride, an inexpensive superhard material. P. Natl. Acad. Sci. USA 108 (27), 10958–10962.

Monkhorst, H.J., Pack, J.D., 1976. Special points for brillouin-zone integrations. Phys. Rev. B 13, 5188–5192.

Mori, T., Tanaka, T., 2006. Effect of transition metal doping and carbon doping on thermoelectric properties of YB_{66} single crystals. J. Solid State Chem. 179, 2889–2894.

Niu, H., Wang, J., Chen, X.Q., Li, D., Li, Y., Lazar, P., Podloucky, R., Kolmogorov, A.N., 2012. Structure, bonding and possible superhardness of CrB_4. Phys. Rev. B: Condens. Matter Mater. Phys. 85, 144116.

Oganov, A.R., Chen, J., Gatti, C., Ma, Y., Ma, Y., Glass, C.W., Liu, Z., Yu, T., Kurakevych, O.O., Solozhenko, V.L., 2009. Ionic high-pressure form of elemental boron. Nature 457, 863–867.

Oku, T., Carlsson, A., Wallenberg, L.R., Malm, J.O., Bovin, J.O., Higashi, I., Tanaka, T., Ishizawa, Y., 1998. Digital HREM imaging of yttrium atoms in YB_{56} with YB_{66} structure. J. Solid State Chem. 135, 182–193.

Oliver, D.W., Brower, G.D., 1971. Growth of single crystal YB_{66} from the melt. J Cryst. Growth 11, 185–190.

Pan, Y., Lin, Y., 2015. Influence of B concentration on the structural stability and mechanical properties of Nb–B compounds. J. Phys. Chem. C 119, 23175–23183.

Parlinski, K., Li, Z.Q., Kawazoe, Y., 1997. First-principles determination of the soft mode in cubic Zr_O2. Phys. Rev. Lett. 78, 4063–4066.

Perdew, J.P., Burke, K., Ernzerhof, M., 1996. Generalized gradient approximation made simple. Phys. Rev. Lett. 77, 3865–3868.

Pugh, S.F., 1954. Relations between the elastic moduli and the plastic properties of polycrystalline pure metals. Philos. Mag. 45, 823–843.

Ravindran, P., Fast, L., Korzhavyi, P.A., Johansson, B., 1998. Density functional theory for calculation of elastic properties of orthorhombic crystals: Application to $TiSi_2$. J. Appl. Phys. 84, 4891–4904.

Richards, S.M., Kaspar, J.S., 1969. The crystal structure of YB_{66}. Acta Crystallogr., Sect. B: Struct. Crystallogr. Cryst. Chem. 25, 237–251.

Romero, M., Benitez-Rico, A., Arévalo-López, E.P., Gómez, R.W., Marquina, M.L., Rosas, J.L., Escamilla, R., 2019. First-principles calculations of the structural, elastic, vibrational and electronic properties of YB_6 compound under pressure. Eur. Phys. J. B 92, 159.

Sauerschnig, P., Vaney, J.B., Michiue, Y., Kouzu, K., Yamasaki, T., Okada, S., Yoshikawa, A., Shishido, T., Mori, T., 2020. Thermoelectric and magnetic properties of spark plasma sintered REB_{66} (RE = Y, Sm, Ho, Tm, Yb). J. Eur. Ceram. Soc. 40, 3585–3591.

A. Savin, O. Jepsen, J. Flad, O.K. Andersen, H. Preuss, H.G.v. Schnering, Electron localization in solid-state structures of the elements: the diamond structure, Angew. Chem., Int. Ed. Engl 31 (1992) 187–188.

Seybolt, A.U., 1960. An exploration of high boron alloys. Trans. ASM 52, 971.

Shein, I.R., Ivanovskĭ, A.L., 2003. Band structure of superconducting dodecaborides YB_{12} and ZrB_{12}. Phys. Solid State 45 (8), 1429–1434.

Song, Y., Wu, X., Hu, B., Ni, D., 2001. Growth of single crystals of YB_2 by a flux method. J. Cryst. Growth 223, 111–115.

Spedding, F.H., Hanak, J.J., Daane, A.H., 1961. High temperature allotropy and thermal expansion of the rare earth metals. J. Less-Common Met. 3, 110–124.

Sun, W., Kuang, X., Keen, H.D.J., Lu, C., Hermann, A., 2020. Second group of high-pressure high-temperature lanthanide polyhydride superconductors. Phys. Rev. B 102, 144524.

Tanaka, T., Okada, S., Yu, Y., Ishizawa, Y., 1997. A new yttrium boride: YB_{25}. J. Solid State Chem. 133, 122–124.

Tateishi, I., Cuong, N.T., Moura, C.A.S., Cameau, M., Ishibiki, R., Fujino, A., Okada, S., Yamamoto, A., Araki, M., Ito, S., Yamamoto, S., Niibe, M., Tokushima, T., Weibel, D.E., Kondo, T., Ogata, M., Matsuda, I., 2019. Semimetallicity of free-standing hydrogenated monolayer boron from MgB_2. Phys. Rev. Mater. 3, 024004.

Tian, Y., Xu, B., Zhao, Z., 2012. Microscopic theory of hardness and design of novel superhard crystals. Int. J. Refract Met. H. 33, 93–106.

Togo, A., Oba, F., Tanaka, I., 2008. First-principles calculations of the ferroelastic transition between rutile-type and $CaCl_2$-type SiO_2 at high pressures. Phys. Rev. B 78, (13) 134106.

Villars, P., Cenzual, K., 2007. Pearson's Crystal Data Crystal Structure Database for Inorganic Compounds. Materials Park, OH, ASM International.

Wang, Y., Lv, J., Zhu, L., Ma, Y., 2010. Crystal structure prediction via particle-swarm optimization. Phys. Rev. B 82, 094116.

Wang, Y., Lv, J., Zhu, L., Ma, Y., 2012. CALYPSO: a method for crystal structure prediction. Comput. Phys. Commun. 183, 2063–2070.

Wang, J., Song, X., Shao, X., Gao, B., Li, Q., Ma, Y., 2018. High-pressure evolution of unexpected chemical bonding and promising superconducting properties of Y_B6. J. Phys. Chem. C 122, 27820–27828.

Wang, W., Zhang, C., Jin, Y., Li, S., Zhang, W., Kong, P., Xie, C., Du, C., Liu, Q., Zhang, C., 2020. Structural, mechanical and electronic properties and hardness of ionic vanadium dihydrides under pressure from first-principles computations. Sci. Rep.-UK 10, 8868.

Waškowska, A., Gerward, L., Olsen, J.S., Babu, K.R., Vaitheeswaran, G., Kanchana, V., Svane, A., Filipov, V.B., Levchenko, G., Lyaschenko, A., 2011. Thermoelastic properties of ScB_2, TiB_2, YB_4 and HoB_4: Experimental and theoretical studies. Acta Mater. 59, 4886–4894.

Weinberger, M.B., Levine, J.B., Chung, H.Y., Cumberland, R.W., Rasool, H.I., Yang, J.M., Kaner, R.B., Tolbert, S.H., 2009. Incompressibility and hardness of solid solution transition metal diborides: $Os_{1-x}Ru_xB_2$. Chem. Mater. 21 (9), 1915–1921.

Wu, Z., Zhao, E., Xiang, H., Hao, X., Liu, X., Meng, J., 2007. Crystal structures and elastic properties of superhard Ir_N2 and Ir_N3 from first principles. Phys. Rev. B 76, 054115.

Xu, Y., Zhang, L., Cui, T., Li, Y., Xie, Y., Yu, W., Ma, Y., Zou, G., 2007. First-principles study of the lattice dynamics, thermodynamic properties and electron-phonon coupling of YB_6. Phys. Rev. B 76, 214103.

Zaykoski, J.A., Opeka, M.M., Smith, L.H., Talmy, I.G., 2011. Synthesis and characterization of YB_4 ceramics. J. Am. Ceram. Soc. 94 (11), 4059–4065.

Zhang, J. Qin, J. Ning, X. Sun, X. Li, M. Ma, R, Liu, First principle study of elastic and thermodynamic properties of FeB_4 under high pressure, J. Appl. Phys. 114 (2013) 183517.

Zhang, J., Jin, Y., Zhang, C., Wang, Y., Tang, L., Li, S., Ju, M., Wang, J., Sun, W., Dou, X., 2022. The crystal structures, phase stabilities, electronic structures and bonding features of iridium borides from first-principles calculations. RSC Adv. 12, 11722–11731.

Zhang, R.F., Legut, D., Lin, Z.J., Zhao, Y.S., Mao, H.K., Veprek, S., 2012. Stability and strength of transition-metal tetraborides and triborides. Phys. Rev. Lett. 108, 255502.

Zhang, C., Sun, G., Wang, J., Lu, C., Jin, Y., Kuang, X., Hermann, A., 2017. Prediction of novel high-pressure structures of magnesium niobium dihydride. ACS Appl. Mater. Interfaces 9, 26169–26176.

Zhang, X., Trimarchi, G., Zunger, A., 2009. Possible pitfalls in theoretical determination of ground-state crystal structures: the case of platinum nitride. Phys. Rev. B 79, 092102.

Zhao, C., Duan, Y., Gao, J., Liu, W., Dong, H., Dong, H., Zhang, D., Oganov, A.R., 2018. Unexpected stable phases of tungsten borides. Phys. Chem. Chem. Phys. 20, 24665–24670.

Zhao, W.J., Xu, B., 2012. First-principles calculations of MnB_4, TcB_4, and ReB_4 with the MnB_4-type structure. Comp. Mater. Sci. 65, 372–376.

Zhou, Y., Liu, B., Xiang, H., Feng, Z., Li, Z., 2015. YB_6: a 'Ductile' and soft ceramic with strong heterogeneous chemical bonding for ultrahigh-temperature applications. Mater. Res. Lett. 3, 210–215.